

# Microstructures and mechanical behavior of bulk nanocrystalline $\gamma$ -Ni-Fe produced by a mechanochemical method

X.Y. Qin<sup>a)</sup>

Laboratory of Internal Friction and defects in Solids, Institute of Solid State Physics Academia Sinica, 230031 Hefei, People's Republic of China

J.S. Lee and C.S. Lee

Department of Metallurgy and Material Science, Hanyang University, 425-791 Ansan, Korea

(Received 5 January 2001; accepted 5 February 2002)

The microstructures and mechanical behavior of bulk nanocrystalline  $\gamma$ -Ni- $x$ Fe (n-Ni-Fe) with  $x = \sim 19$ – $21$  wt%, synthesized by a mechanochemical method plus hot-isostatic pressing, were investigated using microstructural analysis [x-ray diffraction, energy-dispersive spectroscopy, light emission spectrum, atomic force microscopy (AFM), and optical microscopy (OM)], and mechanical (indentation and compression) tests, respectively. The results indicated that the yield strength ( $\sigma_{0.2}$ ) of n-Ni-Fe ( $d \sim 33$  nm) is about 13 times greater than that of conventional counterpart. The change of yield strength with grain size was basically in agreement with Hall-Petch relation in the size range (33–100 nm) investigated. OM observations demonstrated the existence of two sets of macroscopic bandlike deformation traces mostly orienting at  $45$ – $55^\circ$  to the compression axis, while AFM observations revealed that these bandlike traces consist of ultrafine lines. The cause for high strength and the possible deformation mechanisms were discussed based on the characteristics of microstructures and deformation morphology of n-Ni-Fe.

## I. INTRODUCTION

Nanocrystalline materials (n-material)—i.e., polycrystalline materials with grain size smaller than 100 nm—are of considerable scientific and technological interest at present.<sup>1,2</sup> Since the early days of the research in this field, mechanical properties of n-materials have aroused much attention due to their extremely fine grain sizes and large volume fraction (5–50%) of interfaces, which may lead to different and/or improved mechanical properties, such as high strength in n-metals<sup>3</sup> and high ductility in n-ceramics.<sup>4</sup> In the meantime, some contradictory results in the mechanical behavior have been reported. For instance, some investigators reported that normal Hall-Petch (H-P) relation existed<sup>5–9</sup>; while others reported that inverse H-P relations (hardness decreased with decreasing grain size) were found in some n-materials.<sup>10–12</sup> Even hardening and softening behavior on decreasing grain size were found to coexist in some n-materials.<sup>13–15</sup> In recent work, the relationship between Vickers hardness and yield stress in n-Cu was found to be different from that in conventional polycrystalline materials.<sup>16</sup> In view of most earlier work (for example, Ref. 15), we believe

that the main cause of conflicting results or uncertainty (Refs. 5, 13, 17, and 18) in experimental phenomenon lies in difficulties in manufacturing large, dense, and (geometrically) standard specimens for conventional mechanical tests. Hence, to extract intrinsic mechanical behavior and acquire deformation mechanisms of n-materials, it is significant for one to prepare fully dense n-material and to perform mechanical tests with conventional test methods on standard specimens.

In this paper, we report our investigations on microstructures and mechanical behavior of bulk nanocrystalline  $\gamma$ -Ni-Fe (n-Ni-Fe) with  $x \sim 19$  to 21 wt%, synthesized by a mechanochemical process plus hot isostatic pressing (HIPing).  $\gamma$ -Ni- $x$ Fe with  $x = 10$  to 65 wt%, so called Permalloy, is an important material with wide applications in industry.<sup>19</sup> Many techniques have been used to prepare nanocrystalline Ni- $x$ Fe, mostly in powder state.<sup>14,20–24</sup> However, microstructures and mechanical properties of bulk n-Ni-Fe with nearly full density were rarely reported.<sup>14</sup> The synthetic method used here has been shown to be an effective method that has the advantage of producing nano-powders with large quantity and light agglomeration.<sup>24</sup> HIPing is one effective route for consolidating powder into bulk material in relatively low temperature and short time and thus is beneficial to retaining nanophase microstructures.<sup>25</sup> Microstructures and deformation features were characterized

<sup>a)</sup>Address all correspondence to this author.  
e-mail: xyqine@mail.issp.ac.cn

using various methods including x-ray diffraction (XRD), dispersive x-ray spectroscopy (EDS), light emission spectrum (ES), atomic force microscopy (AFM), and optical microscopy (OM). Both conventional Vickers hardness and compression tests were used to characterize mechanical behavior.

## II. EXPERIMENTAL

### A. Synthesis of n-Ni-Fe powder

The powders of n-Ni-Fe alloy were synthesized by a mechanochemical process.<sup>26,28</sup> Experimental details have been given elsewhere.<sup>26</sup> Briefly, the dry mixed oxide powder was obtained by blending  $\alpha$ -Fe<sub>2</sub>O<sub>3</sub> (30  $\mu$ m, 99.99%) and NiO (4  $\mu$ m, 99.99%). Then these dry mixed oxides were ball milled in methyl alcohol at a speed of 300 rpm for 10 h. The ball media and impeller used were made of stainless steel. After ball milling they were dried and sieved. The milled oxides were then reduced at 500 °C for 1 h and then at 550 °C for 0.5 h in hydrogen to create Ni-Fe powder.

### B. Preparation of the bulk material

The obtained Ni-Fe powder was then compacted under uniaxial pressure of approximately 900 MPa into rectangular bars with dimensions of 24  $\times$  8  $\times$  approximately 3 mm<sup>3</sup> (labeled K) and 24  $\times$  8  $\times$  approximately 1.5 mm<sup>3</sup> (labeled T). They had a green (fraction) density of 60–65%. These raw bars were then presintered at 650 °C for 1.5 h in H<sub>2</sub> to remove any oxide present. High-density bars were prepared by HIPing in Bodycote IMT GmbH, Essen, Germany. To do this, the presintered bars were embedded in high-purity Al<sub>2</sub>O<sub>3</sub> powder sealed in an evacuated stainless can (see Fig. 1) and then pressed at 750 °C for 1 h under the pressure of 190 MPa in Ar atmosphere.

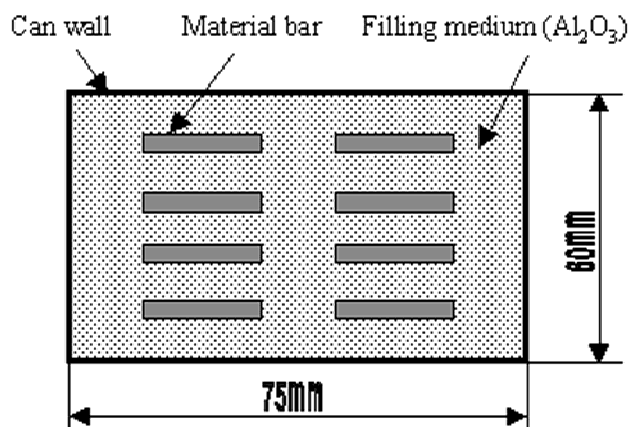


FIG. 1. Schematic drawing showing the placement of the bars in the sealed stainless steel can to be used for hot-isostatic pressing.

### C. Processing of specimens for mechanical testing and surface observation

To carry out compression tests, strip shaped specimens were cut from HIPed bars (K series) in the transverse direction with a spark erosion machine. To avoid the effect of surface damage by the spark erosion and to reduce surface flaws, after cutting, a layer of more than approximately 0.1 mm in thickness was polished away from all sides of the as-machined specimens first with grinding papers (the final was No. 800# paper) and then with diamond pastes (the final had a particle size of 1  $\mu$ m). Unless otherwise mentioned, specimen length is usually 3 times larger than the largest the cross dimension (typical dimensions were approximately 6.2  $\times$  2  $\times$  2 mm<sup>3</sup> after final polishing) to maintain a free deformation section (to avoid the frictional constraints from both ends) in the specimen tested. To observe defects and deformation traces on specimens with OM and AFM, one lateral surface was further specially polished using diamond paste of particle size ¼  $\mu$ m and then etched with Nital (3% HNO<sub>3</sub> + 97% alcohol) for 15 s. There was no surface processing after deformation.

### D. Microstructural characterization

The crystalline structure of the bulk bars was checked using XRD. Also, the mean grain size was determined with XRD based on the Scherrer formula. Well-annealed Si powder was used for the calibration of instrumental broadening. The bar densities were measured based on the Archimedes principle with an accuracy of  $\pm$ 0.2%. A piece of polycrystalline Ni (with purity of 99.99%) annealed at 800 °C for 18 h was used for checking the reliability of density measurements.

Main constituents (Ni, Fe) and their line distributions and spot analysis (including Cr) were determined with EDS. Impurities were analyzed with ES. AFM was used for the evaluation of grain size and its distribution on the specially polished surfaces. In addition, OM and AFM were used to observe the specially polished specimen surfaces before and after deformation (or indentation) to reveal any defects and deformation traces.

### E. Mechanical tests

Compression tests were conducted at room temperature using an Instron type testing machine (Model: Instron 1195) operating at constant rate of anvil displacement. To avoid indenting anvil heads and increase the accuracy in reading yield strength, two well-machined hard-metal plates were placed between the specimen ends and the anvil heads. MoS<sub>2</sub> powder was sprayed in the plates for lubrication. The initial strain rate was approximately  $1.4 \times 10^{-4} \text{ s}^{-1}$ . To investigate the effect of grain size of the material on mechanical behavior (yield

strength and hardness) a series of specimens cut from the same bulk bar were isothermally annealed at 850 °C for different time in sealed quartz tubes filled with argon. Vickers hardness tests were performed with a conventional hardness tester on the specially polished surfaces at room temperature. The applied loads ranged from 3 to 30 kg. An indentation time of 20 s was used in all cases.

### III. RESULTS

#### A. Microstructures and defects

Before HIPing, the crystal structure of all the presintered bars was determined by XRD. The results indicated that a complete gamma phase has already formed similar to the early reports<sup>24</sup> for n-Ni-Fe alloys prepared with the same method (in similar condition) used here. With the line profile analysis in XRD, mean grain size was found to be around 25 nm. Fraction densities  $D_r$  were determined to be in the range of 65–70% (assuming the theoretical density is 8.6 g/cm<sup>3</sup>)<sup>21</sup>.

Table I lists the analytical results of chemical elements for several bars after HIPing. The Fe content was in the range of 19–21 wt%, changing slightly from bar to bar. Apart from the main components (Ni, Fe), there were some impurities, i.e., Cr, Mn, Al, and Si. The Cr content was around 1 wt% (except for K2 and K3 bars), and contents for the other impurity elements were  $\leq 0.1$  wt%. From Table I, one can see that the contents of Fe, Cr, and Mn in bar K2 and K3 were obviously lower than in the other bars. The Al content was nearly same for all the bars. It is worthwhile to note that Si content obtained here with ES had relatively large error since the samples for ES analysis were easily contaminated by dust (silica) from the air when ES measurements were taken, and it is inappropriate to compare the obtained Si content quantitatively.

The density for the bulk bars was greater than 8.3 g/cm<sup>3</sup>, as shown in Table II. Since the materials contained some lighter impurity elements (Al, Si, and Cr, as compared to Ni), the theoretical density  $\rho_0$ , neglecting the possible change in lattice parameter, was estimated to be 8.50–8.56 g/cm. Using this value for  $\rho_0$  one can obtain fraction density of the obtained bulk material to be around 98–99%, as listed in Table II.

TABLE I. Composition of n-Ni-Fe bulk material after HIPing.

Bar	K1	K2	K3	K5	K6	T1
Ni (wt%)	78.4	80.3	79.6	78.2	77.6	78.8
Fe (wt%)	20.6	19.3	19.7	20.6	21.1	20.2
Cr (wt%)	0.8	0.1	0.3	~1	~1	0.8
Mn (wt%)	0.08	0.05	0.05	0.08	0.1	0.08
Al (wt%)	0.03	0.03	0.05	0.03	0.05	0.03
Si (wt%)	0.1	0.05	0.1	0.05	0.05	0.05

TABLE II. Mean grain size  $d$ , density  $\rho$ , fraction density,  $D_r$ , Vickers hardness  $H_v$ , and yield stress  $\sigma_{0.2}$  for several n-Ni-Fe bars after HIPing.

Bar	$d$ (nm)	$\rho$ (g/cm <sup>3</sup> )	$D_r$ (%)	$H_v$ (GPa)	$\sigma_{0.2}$ (GPa)
K1	33	8.34	98.1	5.0 ± 0.1	1.96 ± 0.06
K2	36	8.49	99.2	4.2 ± 0.1	1.59 ± 0.03
K3	34	8.49	99.2	4.2 ± 0.1	1.64 ± 0.03
K5	34	8.31	97.8	4.8 ± 0.1	1.85 ± 0.05
K6	35	8.31	97.8	4.9 ± 0.1	1.94 ± 0.05
T1	38	8.33	98.0	4.6 ± 0.2	1.81 ± 0.05 <sup>a</sup>

<sup>a</sup>Datum obtained by tensile test (details are given in Ref. 27).

Figure 2 gives a typical XRD pattern for n-Ni-Fe after HIPing, where the XRD pattern for pure Ni is also given for the sake of comparison. It can be seen that in addition to the face-centered-cubic (fcc) structure, no other phase was detected. The mean grain size was found from XRD to be around 30–40 nm; the concrete value changed slightly from bar to bar presumably due to different locations within the can used in HIPing experiments. Table II lists some detailed results of grain size for each bar.

Grain size and morphology were investigated using AFM. As an example, Fig. 3 shows an AFM image of grain morphology for a specimen cut from the bar labeled T1. It can be seen from this figure that the grains are fairly homogeneous and largely display spherical shape. Figure 4 gives the histogram of the size distribution obtained by counting the grains according to their sizes. It shows that most of the grains have the size of 30–40 nm, which is in good agreement with XRD results (see Table II).

Figure 5 shows the surface OM micrograph of a specimen cut from bar K5. As expected there was some porosity (labeled A in the graph) in the specimens, consistent with the results of density measurements. Moreover, besides normal porosity some microcracklike defects were occasionally found on the surface as indicated by B in the Fig. 5. However, these microcracklike defects were usually very shallow because they usually disappeared after further polishing. Hence, they can be ascribed to unfinished bonding of the particles (agglomerates of the grains) in HIPing. In addition, from Fig. 5 one can observe some bright regions on the surface, whose typical size is around 50–100  $\mu$ m. They are invisible under OM if they are not etched. Similar patterns existed on the other lateral surfaces, and their main feature (shown in Fig. 5) did not change with different polishing depth, indicating its bulk and particulate character. It is worth noting that grain morphology (size, distribution, or shape) in these bright regions, observed using AFM, has no detectable difference from that in dark regions. That is, they consist of nano-grains features similar to the one in Fig. 3. However, these bright regions

were found to exhibit better resistance to chemical erosion during etching. Since the specimens had only single phase, these regions cannot be explained as second phase. One possible explanation is that the bright regions could possess higher density than the adjacent area. If this is true, then these denser regions would presumably be related to the hard agglomerates in the powder before compaction.<sup>24</sup> However, experimentally there were difficulties in determining local density changes at such a small scale to justify this explanation. Another explanation is that the regions with bright contrast would have different chemical compositions from that in the surrounding area. The line distributions of three main components for bar K5, for instance, were analyzed with EDS

in an electron microprobe, and shown in Fig. 6. It can be seen that the concentrations of the two main elements Ni and Fe, as well as Cr, fluctuate with distance and have a semi-periodicity of approximately 100  $\mu\text{m}$  in their changes. Qualitatively, this concentration change with distance was consistent with the characteristics of dark-bright contrasts (Fig. 5; it should be noted that the area for the line analysis was not just the same area viewed in Fig. 5). In addition, spot analysis with EDS in SEM revealed that bright regions had slightly higher Cr (also higher Fe) content than the dark regions. This analysis seemed to support the assumption that the different contrast under OM would be related to chemical inhomogeneity.

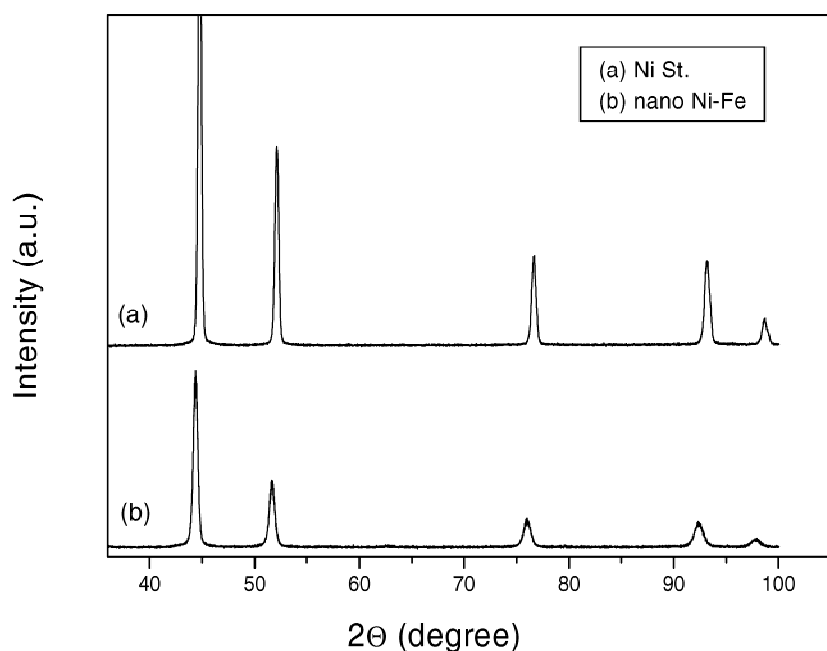


FIG. 2. XRD patterns ( $\text{Cu K}\alpha$  radiation) for (a) a nickel standard and (b) n-Ni-Fe.

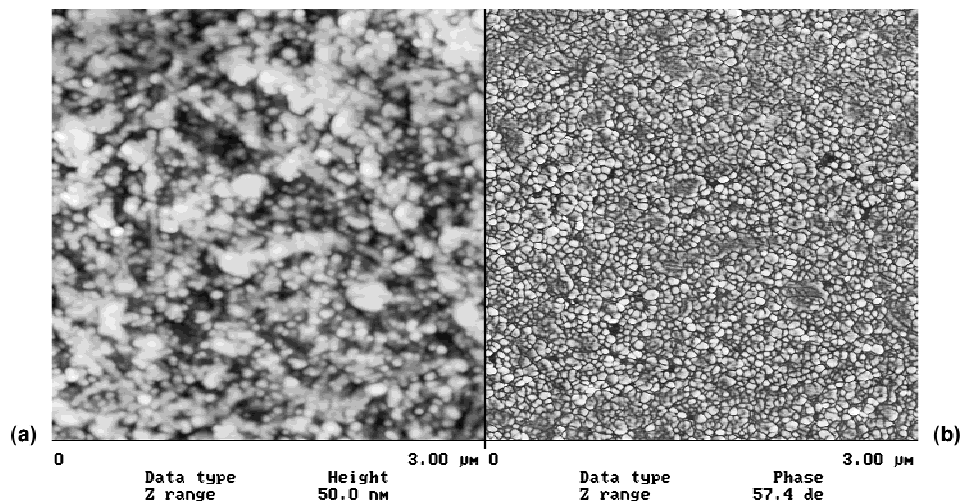


FIG. 3. AFM images for the surface of a specimen cut from bar T1: (a) height image, (b) phase image [it shows the same viewing field as in (a)].

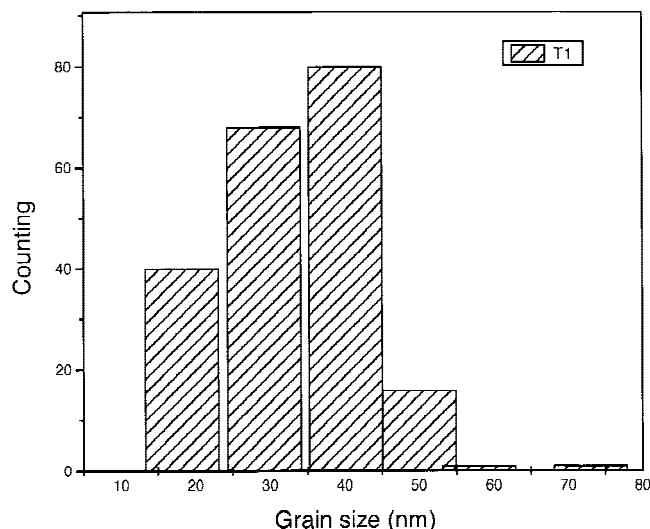


FIG. 4. Distribution of grain size obtained from the AFM images shown in Fig. 3.

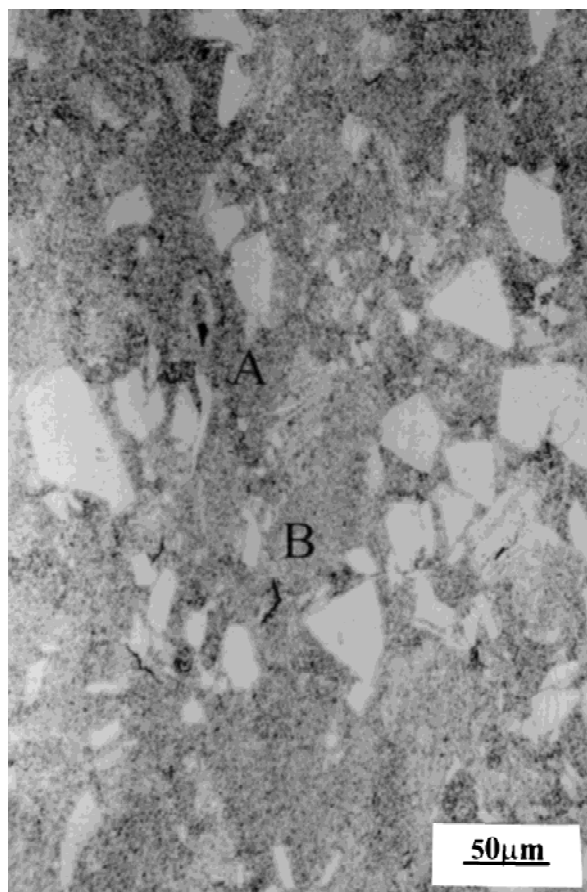


FIG. 5. Micrograph of the surface of a specimen cut from bar K5 observed using an optical microscope. A shows porosity; B shows a microcracklike defect.

## B. Mechanical properties

### 1. Indentation results

Indentation experiments showed that Vickers hardness for the HIPed bulk material ranged from 4.2 to 5.0 GPa, which changed slightly from bar to bar (as given in Table II). The difference in hardness values for different specimens cut from a same bar is usually smaller than 3%. The influences of both measurement number and the applied load on the hardness values were examined. As an example, Fig. 7 gives the plot of the hardness for a specimen cut from K3, obtained under the load of 20 kg, as a function of measurement number. It can be seen that under this load, the average value of its hardness was  $4234 \pm 158$  MPa. The amplitude of the datum fluctuation around its average value was usually smaller than 5%. In addition, experiments showed that hardness did not change obviously with the load as load  $P > 10$  kg. When

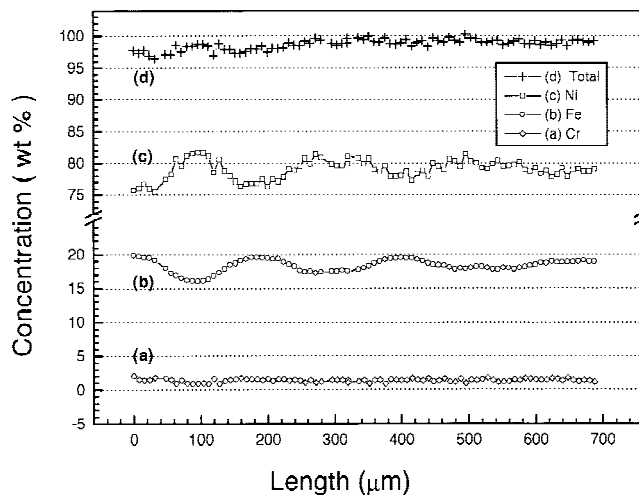


FIG. 6. Line distribution for the three main components Ni, Fe, and Cr. The other impurity elements were neglected in this analysis.

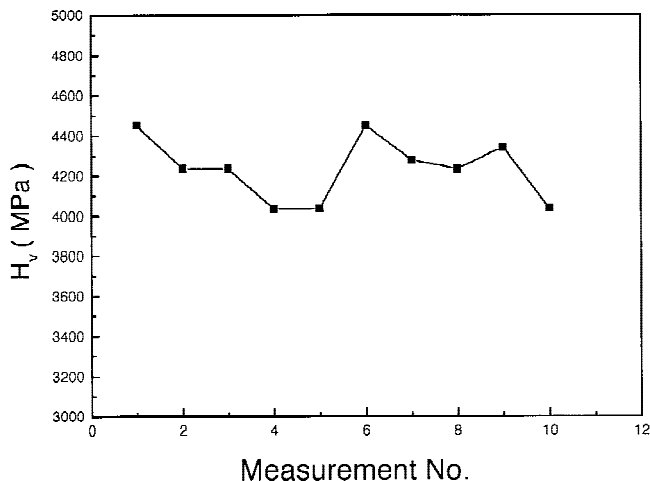


FIG. 7. Vickers hardness for a specimen cut from bar K3 versus measurement number (applied load, 20 kg).

the load was smaller than 10 kg (3 kg, for instance), however, there was a clear tendency that the hardness decreased with decreasing load (see Fig. 8), suggesting that too small load (here <10 kg) would cause large error in determining the hardness.

## 2. Compression results

Figure 9 gives engineering stress–strain curves for K1 series specimens in the as-prepared and annealed states. It can be seen that the flow stress for the as-HIPed specimen decreased after plastic deformation of approximately 0.3%. For the annealed specimens, the strain was slightly larger upon drop of the stress. This decrease in flow stress was caused by bend of the specimens due to their great aspect ratio (length/cross dimension). Yield strength ( $\sigma_{0.2}$ ) for the as-HIPed specimen was obtained from curve (a) to be 1.96 GPa. This value was used to represent the yield stress of the bulk material from which the specimens were cut. The corresponding values for other bulk material (bars) are listed in Table II. It can be seen that the yield strength ranged from 1.59 to 1.96 GPa. Comparing hardness values with the corresponding yield strength, one could find that the yield strength value is about 12% greater than the hardness value divided by 3, indicating that basically a three-times relationship between the hardness value and yield strength held in the n-Ni-Fe. Usually Vickers hardness  $H_V$  is about three times greater than yield stress  $\sigma_{0.2}$ . That is, there is relation  $H_V = 3\sigma_{0.2}$ .

To observe the flow behavior in the large strain range, nonstandard specimens with smaller aspect ratio had to be used to avoid bending too soon. Figure 10 gives the stress–strain curves for two K3 specimens, in which curve (a) is the engineering stress–strain curve for a standard specimen, and curves (b) and (c) were stress–strain curves for a nonstandard one (dimension  $2 \times 2 \times 3 \text{ mm}^3$ ). It can be seen from curve (c) that after complete yielding

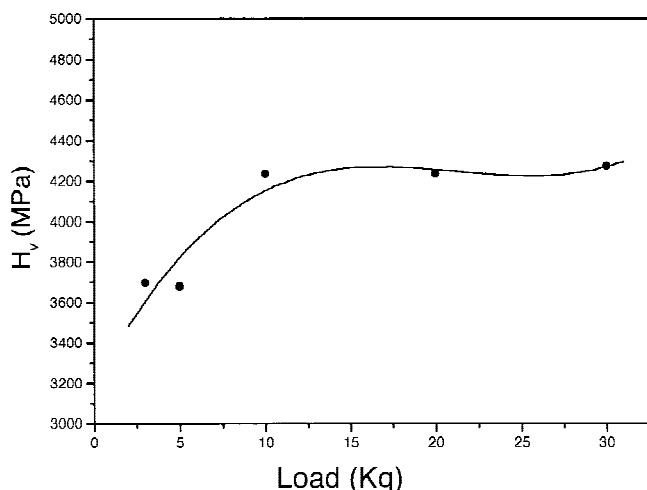


FIG. 8. Vickers hardness of a specimen cut from bar K3 as a function of applied load in indentation.

(the peak stress) there was hardly strain hardening. This result is similar to the early reports on n-Fe-28Al-2Cr.<sup>28</sup> Besides, after the specimen deformed plastically to the strain >15%, no fracture was found. The yield stress ( $\sigma_{0.2}$ ) obtained from this nonstandard specimen [see curves (b) and (c)] was 1.7 GPa, that is, about 6% higher than that (1.6 GPa) from the standard specimen [see curve (a)], indicating the influence of the constraining effect of the anvil heads.

The effect of annealing on the mechanical property of the n-Ni-Fe can be clearly seen in Fig. 9. Figure 11 gives yield strength ( $\sigma_{0.2}$ ) and hardness as a function of annealing time, which shows that yield strength or hardness

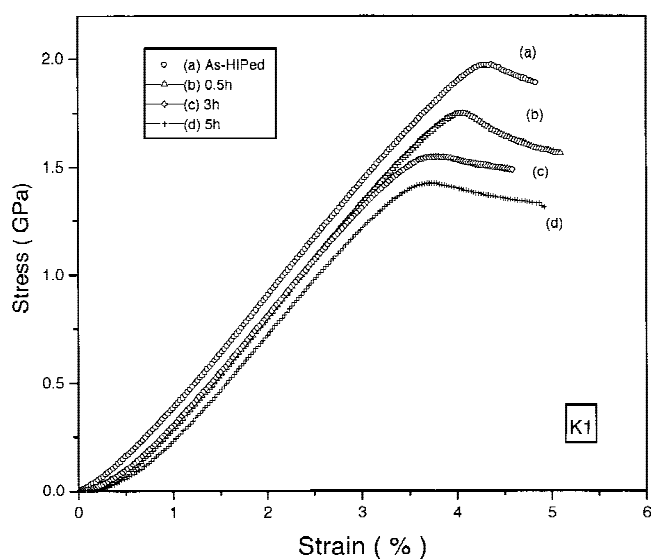


FIG. 9. Engineering stress–strain curves for K1 series specimens in the as-HIPed state (a), and annealed at 850 °C for (b) 0.5 h, (c) 3 h, and (d) 5 h.

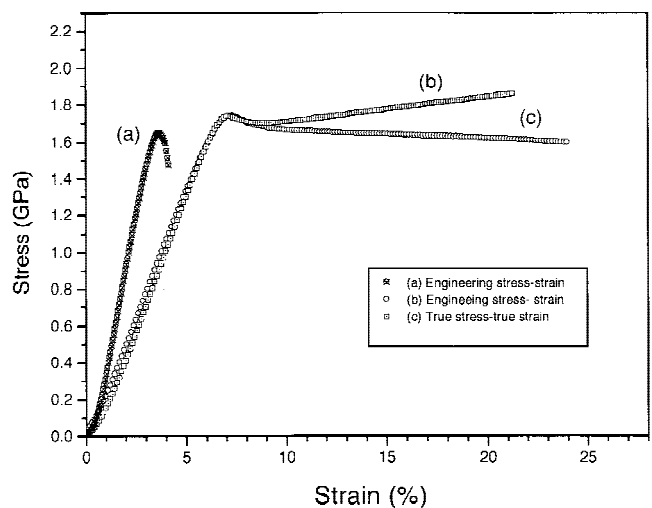


FIG. 10. Stress–strain curves for two K3 specimens: (a) engineering stress–strain curve for a standard specimen, (b) engineering stress–strain curve for a nonstandard specimen, (c) true stress–strain curve for the nonstandard specimen.

decreased monotonously with increasing annealing time. This decrease in strength can be reasonably ascribed to growth of its grain size. Figure 12 shows the plot of the yield stress versus  $d^{-1/2}$ . For comparison, the hardness values divided by three is also given in the figure. It can be seen that basically a straight line between yield stress and  $d^{-1/2}$  can be drawn. By best fit of the data to H-P relation, friction stress  $\sigma_0 = 0.70$  GPa and slope  $k = 7.0$  GPa ( $\text{nm}^{1/2}$ ) were obtained. There was a similar linear relation between hardness and  $d^{-1/2}$ .

### C. Deformation morphology

Light OM observations on the specimen surface after indentation indicated that there were some plastic areas (pileups) around indentation traces similar to the case of n-Fe with grain size  $d > 20$  nm.<sup>29</sup> Figure 13 shows this observation for a specimen cut from K3. In all the indentation tests no crack was observed around the indentation traces (see Fig. 13). Even for the largest

load (30 kg) applied, no cracks were found near the indentation corners where the indenter produced considerable tensile stresses, as shown in Fig. 14. In this case, the deformed area (pileup) extended to over 100  $\mu\text{m}$  away from the indentation. In addition, the plastically deformed area did not appear to be smooth; rather its surface looked very rugged, implying deformation localization.

After compression tests were stopped (usually with nominal strain of 1–3%), OM was used to check the deformation traces. Observations indicated that usually relatively few deformed traces could be found in the central parts of the specimens. In contrast, a large number of deformation traces existed near both ends of the compressed specimens. Figure 15 shows a typical OM micrograph of surface morphology. It can be seen that the deformation has the characteristic of high heterogeneity. However, the striking feature of the morphology was the formation of two sets of macroscopic bandlike traces (BLTs) that were symmetric to load axis and mostly oriented at 45–55° to the compression axis.

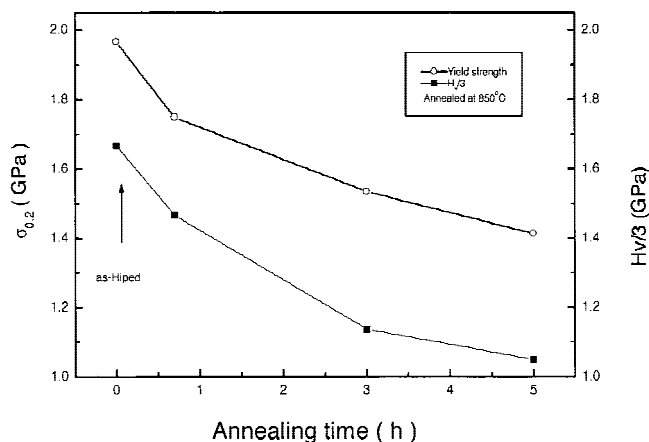


FIG. 11. Plot of yield strength and the hardness (divided by 3) versus time of isothermal annealing at 850 °C.

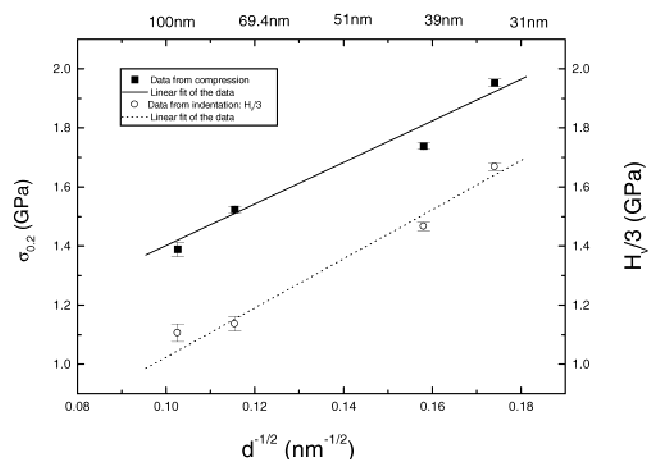


FIG. 12. Plot of yield strength and hardness (divided by 3) versus  $d^{-1/2}$ . Solid and open circles are experimental data, and the straight lines (solid and dot) are the corresponding linear fits to the data.

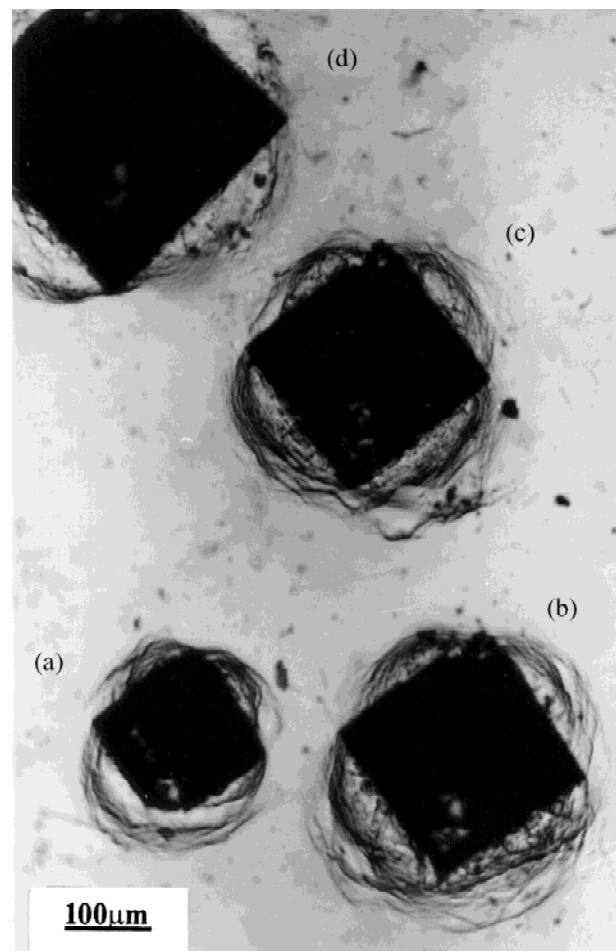


FIG. 13. Optical micrograph of Vickers indentations: (a) indentation load, 10 kg; (b) and (c) indentation load, 20 kg; (d) indentation load, 30 kg.

Figure 16 shows an AFM image for the same deformation traces. In this magnification (image size  $40 \times 40 \mu\text{m}$ ), the BLTs constituted parallelogramic networks on the specimen surface. Figure 17 gives an AFM image with higher magnification. In this image, grain contours are faint, but they are resolvable. Specially, one can see clearly a great number of sharp (with most of their transverse dimensions being clearly smaller than grain sizes) and long nanochannels or grooves, demonstrating ultra-fine structures of BLTs (Figs. 15 and 16). Due to limitations of the spatial resolution (approximately 15 nm) of AFM, it is difficult to resolve if deformation happened within the individual nano-grains (approximately 30 nm). Nevertheless, from close inspection of the image it could be seen that most of the sharp channels seemed to run between the grains, implying deformation took place mainly in grain boundary regions.

#### IV. DISCUSSIONS

##### A. Yield strength and hardness of n-Ni-Fe

In this study, very high values of yield strength and hardness ( $\sigma_{0.2} = 1.54$  to  $1.96$  GPa and  $H_v = 4.2$  to  $5.0$  GPa) were obtained for n-Ni-Fe alloy. These values of yield

strength are about 13 times greater than the literature values (150 MPa) for the permalloy with similar Ni content,<sup>30</sup> and even greater than that (approximately 1.4 GPa) of high-strength steels.<sup>31</sup> This great yield strength can be explained reasonably in terms of the refinement of the grains in the specimens because the

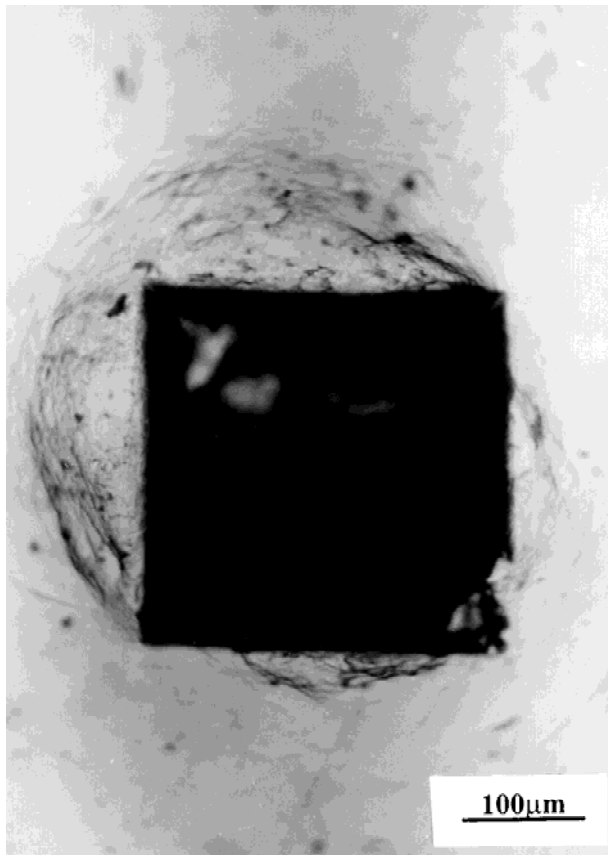


FIG. 14. Magnified micrograph of Vickers indentations under a load of 30 kg.

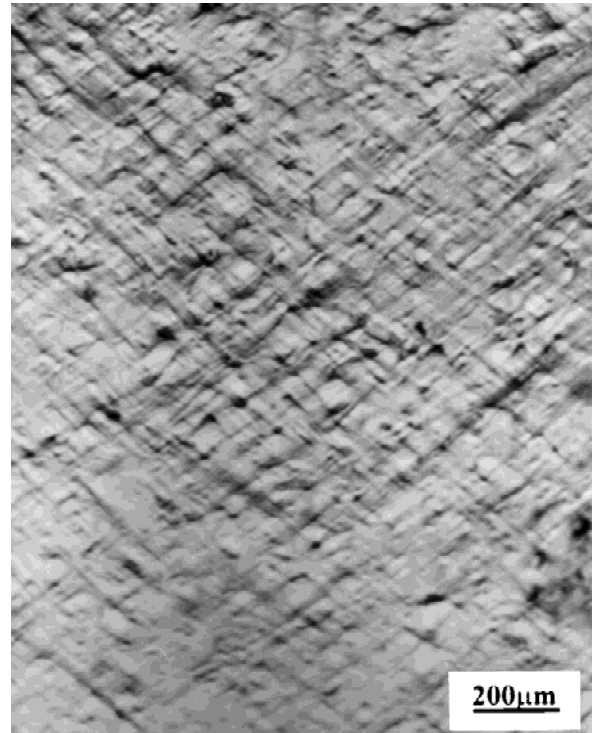


FIG. 15. Optical micrograph of a lateral surface for a specimen cut from bar K3 after compression. The direction of compression axis is vertical.

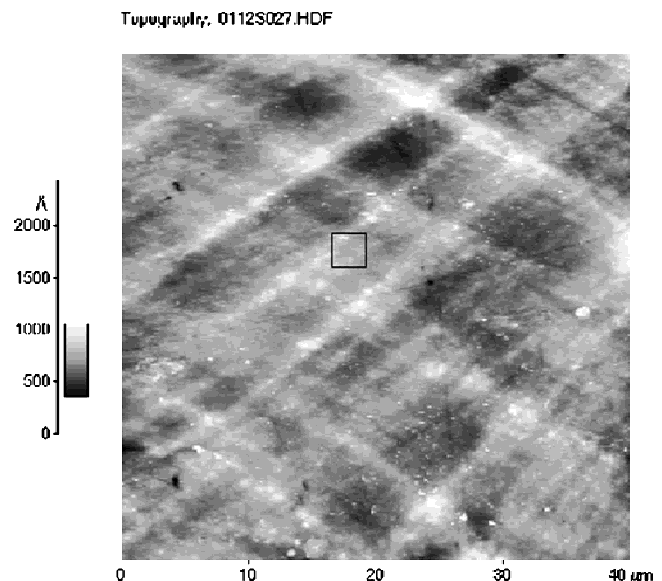


FIG. 16. AFM image of the compressed specimen surface (image size:  $40 \times 40 \mu\text{m}$ ). The direction of compression axis is vertical.

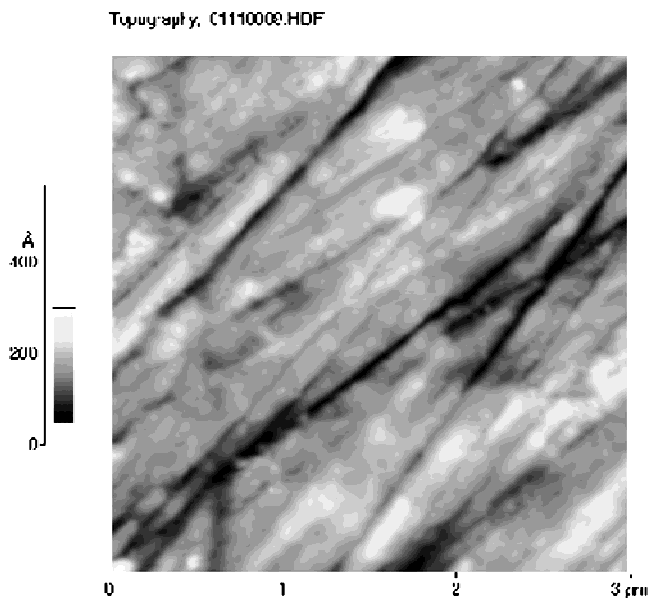


FIG. 17. AFM image with high magnification (image size:  $3 \times 3 \mu\text{m}$ ). The viewing field is shown by the square in Fig. 16. The direction of compression axis is vertical.

hardening effect of grain refinement has been demonstrated clearly in Fig. 12. It is worthwhile to note that the hardness of n-Ni-Fe obtained here is higher than early results.<sup>15</sup> In the n-Ni-Fe alloy synthesized by electrodeposition, a hardness value of about 3.2 GPa can be obtained if their results are linearly extrapolated to the grain size of approximately 30 nm.<sup>15</sup> The lower strength for their n-Ni-Fe would originate from the existence of the texture in the material<sup>15</sup> because as their experiments indicated, microtexture formed in specimens during electrodeposition. The existence of this texture would lead to softening of the material due to easy transfer of dislocations from one grain to another with a similar orientation. In contrast, no evidence of texture in our specimens was revealed by XRD (see Fig. 2).

The difference in strength (or hardness) among different bars should be related to the difference in their microstructures. This may include the following:

(i) **Densification:** The fraction density (99.2%) of bar K2 and K3 was about 1% higher than that of the others, while both yield stresses were obviously smaller than those of the others. Normally the higher the densification of n-material, the greater its strength would be.<sup>9</sup> Hence, the difference in strength could hardly be explained based on density difference. One point that should be noted is that there was some error in the calculations of the fraction densities listed in Table II since the actual theoretic density will change with chemical compositions of an alloy. Concretely speaking, the Ni content in bar K2 and K3 was obviously higher than that in the others. Correspondingly, the theoretic density for K2 and K3 would be higher than that of others due to the greater atomic weight of nickel. In other words, the actual difference

in densification among different bars would be smaller than 1%. The effect of this small densification difference on strength could be negligibly small as compared to other factors (see following context).

(ii) **Chemical composition:** As compared to bar K2 and K3 with lower yield strength, the contents of Fe, Cr, and Mn in the other bars were clearly higher. The higher contents of these alloying (impurity) elements would cause the material to become harder through solid solution strengthening mechanism.

(iii) **Local inhomogeneity:** As shown in Fig. 5, there was microstructural inhomogeneity in n-Ni-Fe. Although present experiments did not justify if it came from density fluctuation, chemical fluctuation (Fig. 6) or from both, one thing seemed to be certain was that the regions with bright contrast deformed less (Fig. 15) than other areas during compression, indicating their greater hardness. Their contribution to the total strength of the material would be similar to harder phases within composites. The more its content, the higher the strength of the material as a whole would be. Experimentally there was difficulty in determining the amount and spatial or/and size distributions of the harder aggregates in respective bars. However, if one assumes that the impurity content, such as Cr, was related to (or reflected) the amount of the harder aggregates, the bars with higher alloying (impurity) contents would be harder. Then the different strength (or hardness) among different bars (Table II) can be qualitatively explained.

## B. Deformation mechanism

As shown in Fig. 12, the stress increased with decreasing grain size, basically consistent with a normal H-P relation. In other words, this means that the strengthening effect due to grain size refinement functioned in this grain size range (33–100 nm). Similar strengthening effect by grain size was obtained recently in n-Cu<sup>32</sup> and n-Fe.<sup>29</sup> According to dislocation theory<sup>33</sup> and Taylor theory,<sup>34</sup> the critical normal stress  $\sigma$  for dislocation generation is  $\sigma \approx m\tau \approx 3Gb/L$  (here  $\tau$  is the critical shear stress,  $G$  shear modulus,  $b$  the Burgers vector,  $L$  the length of dislocation segment, and  $m \approx 3.06$  orientation factor). In a n-material, the length of a dislocation should be constrained by grain size. That is, there is a relation  $L \leq d$  (here  $d$  is grain size). As a qualitative evaluation, substituting  $b = 0.25 \text{ nm}$  for Ni,<sup>35</sup>  $G = 78 \text{ GPa}$ ,<sup>30</sup> and  $d = 33 \text{ nm}$  into formula (2),  $\sigma = 1.81 \text{ GPa}$  is obtained. This value coincides well with the yield stress of n-Ni-Fe in the as-HIPed state [see curve (a) in Fig. 9 and Table II]. This evaluation suggests that multiplication of dislocations with the length of the grain sizes could occur in n-Ni-Fe. The existence of a large number of sharp, long, and fairly straight nano-channels revealed with AFM (Fig. 17) might be explained by traces of dislocation motion, i.e., “slip lines.” However, since no

deformation within individual nano-grains was resolved (perhaps due to the limitation of AFM resolution), the dislocation activity, if any, could more likely be related to grain boundary (GB) dislocations because most of channels seemed to run through in between the grains (Fig. 17). Very recently, the present authors found that the strain-rate sensitivity exponent for n-Ni-Fe was  $n = 0.01$  at room temperature,<sup>36</sup> which excluded possibility of normal GB sliding mechanism, for  $n$  is usually near 0.5 as GB sliding prevails. Other investigations showed that GB sliding occurred as homologous temperature ( $T/T_m$ )  $> 0.36$  on n-Ni<sup>37</sup> and n-Mg.<sup>38</sup> Hence, it seems unlikely that GB sliding would occur here at room temperature [approximately  $0.18 T_m$ ; here  $T_m$  is melting point (approximately 1452 °C) of Ni-Fe]. Therefore, deformation mechanism in n-Ni-Fe at room temperature could still be some kind of dislocation mode.

## V. CONCLUSION

Nano  $\gamma$ -Ni- $x$ Fe ( $x \sim 19$  to 21 wt%) with grain size as small as 33 nm and with fraction density  $D > 98\%$  was synthesized by a mechanochemical method plus hot isostatic pressing. Compression tests revealed that in the grain size range (33–100 nm) investigated, yield stress increased with decreasing grain size, basically in agreement with a normal Hall-Petch relation. Experiments also indicated that the yield strength ( $\sigma_{0.2}$ ) for n-Ni-Fe ( $d \sim 33$  nm) is about 13 times greater than that for the conventional counterpart. OM observations demonstrated the existence of two sets of macroscopic bandlike deformation traces mostly orienting at 45–55° to the compression axis, while AFM observations revealed that these traces consist of nanochannels or ultrafine lines. The great strength or hardness of n-Ni-Fe could be explained as strengthening effect caused by grain boundaries and grain refinement. Microstructural inhomogeneity would mainly be responsible for additional strength difference among respective bulk materials. However, further work is needed to elucidate the deformation mechanism in n-Ni-Fe.

## ACKNOWLEDGMENTS

One author (Qin) gratefully acknowledges the Alexander von Humboldt Foundation for providing a fellowship. He especially wishes to acknowledge Prof. E. Nembach who, as a host professor, contributed much in both arranging facilities for this work and instructing the author to carry out this research. The authors would like to thank the Institut für Metallforschung, Universität Münster for providing all the necessary facilities. In addition, the authors are indebted to Mr. T. Krol for his assistance in mechanical tests, Dr. D. Baither and

Prof. Q.P. Kong for their helpful discussions, and Dr. L.F. Chi, Dr. S. Gao, and Mr. X.G. Zhu for their help in AFM observations as well as Bodycote IMT GmbH, Essen, Germany for HIPing experiments. This work was financially supported partly by Academic Sinica through the Hundred Person Program and the Korean Ministry of Science and Technology through the 2001 National Research Laboratory Program.

## REFERENCES

1. H. Gleiter, *Prog. Mater. Sci.* **33**, 223 (1989).
2. C. Suryanarayanan, *Int. Met. Rev.* **40**, 41 (1995).
3. V.Y. Gertsman, R. Birringer, R.Z. Valiev, and H. Gleiter, *Scripta Metall. Mater.* **30**, 229 (1994).
4. J. Karch, R. Birringer, and H. Gleiter, *Nature* **330**, 556 (1987).
5. G.W. Nieman, J.R. Weertman, and R.W. Siegel, *Scripta Metall. Mater.* **23**, 2013 (1989).
6. J.S.C. Jang and C.C. Koch, *Scripta Metall. Mater.* **24**, 1599 (1990).
7. S.K. Ganapathi and D.A. Rigney, *Scripta Metall. Mater.* **24**, 1675 (1990).
8. H.J. Höfler and R.S. Averback, *Scripta Metall. Mater.* **24**, 2401 (1990).
9. X.Y. Qin, X.J. Wu, and L.D. Zhang, *Nanostruct. Mater.* **5**, 101 (1995).
10. A.H. Chokshi, A. Rosen, J. Karch, and H. Gleiter, *Scripta Metall. Mater.* **23**, 1679 (1989).
11. K. Lu, W.D. Wei, and J.T. Wang, *Scripta Metall. Mater.* **24**, 2319 (1990).
12. T. Christman and M. Jain, *Scripta Metall. Mater.* **25**, 767 (1991).
13. G.E. Fogere, J.R. Weertman, R.W. Siegel, and S. Kim, *Scripta Metall. Mater.* **26**, 1879 (1992).
14. C. Cheung, F. Djuanda, U. Erb, and G. Palumbo, *Nanostruct. Mater.* **5**, 513 (1995).
15. J.R. Weertman, M. Niedzielka, and C. Youngdahl, *Mechanical Properties and Deformation Behavior of Materials Having Ultrafine Microstructures*, edited by M. Nastasi, D.M. Parkin, and H. Gleiter (Kluwer, Dordrecht, Germany, 1993), p. 241.
16. P.G. Sanders, J.A. Eastman, and J.R. Weertman, *Acta Mater.* **45**, 4019 (1997).
17. G.W. Nieman, J.R. Weertman, and R.W. Siegel, *J. Mater. Res.* **6**, 1012 (1991).
18. G.W. Nieman, J.R. Weertman, and R.W. Siegel, *Scripta Metall. Mater.* **24**, 145 (1990).
19. *Ferromagnetic Materials*, edited by E.P. Wohlfarth (North-Holland, Amsterdam, The Netherlands, 1980), Vol. 2, p. 123.
20. C. Kuhrt and L. Schultz, *J. Appl. Phys.* **73**, 1975 (1993).
21. F.D. Ge, L.M. Chen, W.J. Ku, and J. Zhu, *Nanostruct. Mater.* **8**, 703 (1997).
22. S. Eroglu, S.C. Zhang, and G.L. Messing, *J. Mater. Res.* **11**, 1231 (1996).
23. Y.H. Zhou, M. Harmelin, and J. Bigot, *Scripta Metall.* **23**, 1391 (1989).
24. X.Y. Qin, J.S. Lee, J.G. Nam, and B.S. Kim, *Nanostruct. Mater.* **11**, 383 (1999).
25. A.S. Helle, K.E. Easterling, and M.F. Ashby, *Acta Metall.* **33**, 2163 (1985).
26. J.S. Lee, T.H. Kim, J.H. Yu, and S.W. Chung, *Nanostruct. Mater.* **9**, 153 (1997).
27. X.Y. Qin, J.S. Lee, and C.S. Lee (unpublished).
28. M. Tain and T. Christman, *Acta. Metall. Mater.* **42**, 1901 (1994).

29. T.R. Malow and C.C. Koch, *Metall. Mater. Trans.* **29A**, 2285 (1998).
30. *Ferromagnetic Materials*, edited by E.P. Wohlfarth (North-Holland, Amsterdam, The Netherlands, 1980), Vol. 2, p. 123.
31. D. Wiliam and J.R. Callister, *Materials Science and Engineering*, 2nd ed. (John Wiley & Sons, New York, 1991), p. 112.
32. V.Y. Gertsman, M. Hoffmann, H. Gleiter, and R. Birringer, *Acta Metall. Mater.* **42**, 3539 (1994).
33. J. Friedel, *Dislocations* (Pergamon Press, London, United Kingdom, 1964), Chap. 8.
34. R.W.K. Honeycombe, *The Plastic Deformation of Metals*, 2nd ed. (Edward Arnold, London, United Kingdom, 1984), p. 227.
35. J. Friedel, *Dislocations* (Pergamon Press, London, United Kingdom, 1964), Appendix B.
36. X.Y. Qin, X.G. Zhu, G. Song, and J.S. Lee, *J. Phys. Condens. Matter* **14**, 2605 (2002).
37. L.I. Trusov, T.P. Khvostantseva, V.A. Solov'ev, and V.A. Mel'nikov, *Nanostruct. Mater.* **4**, 803 (1994).
38. S. Hwang, C. Nishimura, and P.G. McCormick, *Scripta Metall.* **44**, 1507 (2001).